SCIENCE CHINA
Technological Sciences

August 2010 Vol.53 No.8: 2160–2171
doi: 10.1007/s11431-010-4023-3

Fast multipole boundary element analysis of 2D viscoelastic composites with imperfect interfaces

ZHU XingYi[1], CHEN WeiQiu[2], HUANG ZhiYi[1*] & LIU YiJun[3]

[1] *Department of Civil Engineering, Zhejiang University, Zijingang Campus, Hangzhou 310058, China;*
[2] *Department of Engineering Mechanics, Zhejiang University, Yuquan Campus, Hangzhou 310027, China;*
[3] *Department of Mechanical Engineering, University of Cincinnati, Cincinnati, Ohio 45221-0072, USA*

Received January 19, 2010; accepted May 27, 2010

A fast multipole boundary element method (FMBEM) is developed for the analysis of 2D linear viscoelastic composites with imperfect viscoelastic interfaces. The transformed fast multipole formulations are established using the time domain method. To simulate the viscoelastic behavior of imperfect interfaces that are frequently encountered in practice, the Kelvin type model is introduced. The FMBEM is further improved by incorporating naturally the interaction among inclusions as well as eliminating the phenomenon of material penetration. Since all the integrals are evaluated analytically, high accuracy and fast convergence of the numerical scheme are obtained. Several numerical examples, including planar viscoelastic composites with a single inclusion or randomly distributed multi-inclusions are presented. The numerical results are compared with the developed analytical solutions, which illustrates that the proposed FMBEM is very efficient in determining the macroscopic viscoelastic behavior of the particle-reinforced composites with the presence of imperfect interfaces. The laboratory measurements of the mixture creep compliance of asphalt concrete are also compared with the prediction by the developed model.

boundary element method, fast multipole method, viscoelasticity, imperfect interface, multi-inclusion composite

Citation: Zhu X Y, Chen W Q, Huang Z Y, et al. Fast multipole boundary element analysis of 2D viscoelastic composites with imperfect interfaces. Sci China Tech Sci, 2010, 53: 2160–2171, doi: 10.1007/s11431-010-4023-3

1 Introduction

Recent developments in technology, such as gas turbines, jet engines, nuclear power plants and space crafts, have placed severe demands on high performance of materials, especially stability. However, most engineering materials are time-dependent materials. Because of the time-effect, actual materials will possess viscous and elastic properties simultaneously, making practical structures suffer from creep, relaxation and hysteresis problems. Consequently, the time-dependent or viscoelastic behavior of materials has been of great importance. Full understanding of the mechanism and response of viscoelastic materials under external loadings will help us to provide the scientific basis for predicting the service-life of engineering structures or components.

The boundary element method (BEM) is a promising numerical tool for serving this purpose, due to its features of dimensionality reduction and high accuracy. Many investigators have applied BEM to the investigation of viscoelastic characteristics of materials and structures. Along with the BEM, the most commonly used technique is the Laplace transform method [1–4]. By the elastic-viscoelastic correspondence principle [5], the viscoelastic governing equations can be transformed into a set of corresponding elastic governing equations using the Laplace transform. The solutions are then transformed back to the time domain by nu-

*Corresponding author (email: hzy@zju.edu.cn)

merical methods. Mesquita et al. [6–9] presented a boundary element alternative procedure for Boltzmann and Kelvin viscoelasticity based on the assumption of viscoelastic constitutive relations and weighted residual technique. They produced the differential systems of equations with respect to time variable, which were solved by an appropriate time marching process. Combining the approach based on the two-dimensional version of Somigliana's formula with the time-marching procedure described for the viscoelastic analysis by Mesquita et al., Huang et al. [10] considered the problem of an infinite, isotropic viscoelastic plane containing randomly distributed elastic inclusions. Sensale et al. [11–13] transformed the domain integral into a boundary integral using the dual reciprocity method for the stress analysis of bodies with aging viscoelastic constitutive relations. Birgisson et al. [14–16] employed a special boundary element-based method, called the displacement discontinuity method, along with an explicit time-marching scheme, to model the quasi-static response of linear viscoelastic materials.

The numerical methods based on boundary integral equation mentioned above only consider composites with perfect interfaces. Actually, it is inadequate to describe the physical nature and macromechanical behavior of engineering materials, such as fiber-reinforced composites, by considering the bond between matrix and fibers as perfect. However, when the interface is imperfect, additional efforts should be made in the analysis. Lene and Leguillon [17] modeled the interfacial zone by a spring layer with vanishing thickness. It is assumed that the tractions are continuous while jumps of displacements are allowed to cross the interface, and these jumps are proportional to the conjugate tractions transmitted across the interface. Such an interface model is elastic in nature. However, when the composites present apparent viscoelastic characteristic, it will be more suitable to describe the behavior of bond adhesives by means of viscoelastic interfaces. Hence, in the present paper, the Kelvin type model is employed to describe the viscoelastic interfaces. Actual interaction among inclusions and elimination of the phenomenon of material penetration are both taken into consideration.

Analysis of viscoelastic problems often requires multi-time-step computation to predict accurate creep or relaxation behavior of the bodies under external loadings. Besides, an iterative algorithm should be employed to ensure that the material penetration phenomenon will not occur. Therefore, when we are dealing with large-scale models, such as multi-inclusion composites, the computation time and storage space will increase significantly. The conventional boundary element-based method requires $O(N^2)$ operations using iterative solvers (with N being the number of equations) because of its dense and non-symmetrical matrices. Thus conventional BEM-based approach is not suitable for solving large-scale viscoelastic problems with imperfect interfaces. Fast multipole method (FMM) is a new algorithm developed recently for numerical solution of BEM. This algorithm has been proved that it can solve system equations formed by BEM with higher efficiency and lower storage than that of the traditional solvers.

For elasticity problems, there have been a lot of works reported on fast multipole BEM approaches. Greengard et al. [18, 19] developed a fast multipole formulation for directly solving the biharmonic equations using Sherman's complex variables formulae. Peirce and Napier [20] gave a spectral multipole approach similar to the FMMs, reducing the complexities of both memory and operation to $O(N\log N)$. Yao et al. [21] and Wang et al. [22] presented a fast and accurate algorithm for modeling composite materials and crack problems. They applied complex Taylor expansion and adaptive tree structure to obtain a new shift of multipole expansion for two-dimensional elastostatics. Liu et al. [23–25] proposed compact and efficient fast multipole BEM formulations for both 2D and 3D elasticity problems. In Liu's approach for 2D elastostatics [24], the displacement and traction kernels are represented using two complex analytic functions, and the two functions are first re-grouped and then expanded to form two moments for each kernel. In their work, they reduced the CPU time and memory usage in the fast multipole accelerated BEM to $O(N)$. This approach has recently been extended to 2D multi-domain elasticity problems [26]. A systematic description and various applications of the fast multipole BEM can be found in ref. [27]. In our previous study [28], we have developed the formulations of fast multipole BEM for the elastic analysis of composites which accounts for the effect of bonding imperfection between matrix and inclusions.

In this paper, the formulations of fast multipole BEM analysis of 2D viscoelastic composites with imperfect viscoelastic interface are presented. First, the boundary integral equation for 2D viscoelasticity is expressed in the time domain, which is discretized using a special numerical scheme [29]. The multipole expansion formulations are developed. Then, the Kelvin type viscoelastic model is adopted to simulate the interface bonding imperfection. Based on this model, a system of equations for 2D viscoelastic solids containing elastic particles but with in-between viscoelastic interfaces is formulated. Analytical solutions for a single-embedded inclusion and randomly distributed multi-inclusion planar viscoelastic composites with imperfect interfaces are also developed. Numerical results are presented and verified by the analytical solutions, and the accuracy and efficiency of the approach are illustrated. The developed FMBEM is finally used to predict the creep compliance of an asphalt concrete, which is a typical viscoelastic composite. The laboratory measurements of the mixture creep compliance are compared with that predicted by the developed BEM model.

2 FMBEM for 2D viscoelasticity

According to the viscoelastic reciprocity theorem, the boundary integral equation for 2D isotropic viscoelasticity

without body force can be expressed as follows [29,30]:

$$C_{ij}(\boldsymbol{x})u_j(\boldsymbol{x},t)=\int_S\Bigg[U_{ij}(\boldsymbol{x},\boldsymbol{y},0)p_j(\boldsymbol{y},t)+\int_0^t p_j(\boldsymbol{y},t-\tau)\frac{\partial U_{ij}(\boldsymbol{x},\boldsymbol{y},\tau)}{\partial\tau}d\tau\Bigg]\mathrm{d}S(\boldsymbol{y})-\int_S\Bigg[P_{ij}(\boldsymbol{x},\boldsymbol{y},0)u_j(\boldsymbol{y},t)+\int_0^t u_j(\boldsymbol{y},t-\tau)\frac{\partial P_{ij}(\boldsymbol{x},\boldsymbol{y},\tau)}{\partial\tau}d\tau\Bigg]\mathrm{d}S(\boldsymbol{y}),\quad(1)$$

where S is the boundary of domain V_0, which is occupied by the viscoelastic body; $C_{ij}(\boldsymbol{x})$ is a free term determined from the shape of the boundary S at point x; u_i and p_i are the displacements and tractions respectively; P_{ij} and U_{ij} are the fundamental solutions for an infinite viscoelastic body subjected to a Heaviside unit step force, and they can be defined as follows:

$$U_{ij}(\boldsymbol{x},\boldsymbol{y},t)=\frac{1}{8\pi}\Bigg[J_1(t)\delta_{ij}\ln\left(\frac{1}{r}\right)+J_2(t)\left(r_{,i}r_{,j}-\frac{1}{2}\delta_{ij}\right)\Bigg],\quad(2)$$

$$P_{ij}(\boldsymbol{x},\boldsymbol{y},t)=\frac{1}{8\pi r}\Bigg\{J_3(t)\left(r_{,i}n_j-r_{,j}n_i-\frac{\partial r}{\partial n}\delta_{ij}\right)+J_4(t)\Bigg[\frac{\partial r}{\partial n}\left(\delta_{ij}-4r_{,i}r_{,j}\right)+r_{,j}n_i-r_{,i}n_j\Bigg]\Bigg\}.\quad(3)$$

Functions $J_1(t)$, $J_2(t)$, $J_3(t)$ and $J_4(t)$ are called four basic functions, which can be obtained by Laplace inverse transform from their counterparts in the Laplace domain

$$J_j(t)=L^{-1}\left[\tilde{J}_j(s)\right]\quad(j=1,2,3,4).\quad(4)$$

In the following analysis, we assume that the material behaves elastically in dilatation, so that the bulk modulus K is a constant, while the shear modulus $\tilde{G}$ and the Poisson's ratio $\tilde{\nu}$ are time-dependent in general. Therefore, according to the correspondence principle, the functions $\tilde{J}_i(s)$ can be obtained as

$$\tilde{J}_1(s)=\frac{2(3K+7\tilde{G})}{\tilde{G}\left(3K+4\tilde{G}\right)s},\quad(5)$$

$$\tilde{J}_2(s)=\frac{2(3K+\tilde{G})}{\tilde{G}\left(3K+4\tilde{G}\right)s},\quad(6)$$

$$\tilde{J}_3(s)=\frac{2(3K+7\tilde{G})}{(3K+4\tilde{G})s},\quad(7)$$

$$\tilde{J}_4(s)=\frac{2(3K+\tilde{G})}{\left(3K+4\tilde{G}\right)s},\quad(8)$$

with s being the transform parameter. Note that the constitutive equations for a linear viscoelastic material can be written in a differential form as

$$P'S_{ij}=Q'e_{ij},\ \tilde{G}=\frac{Q'(s)}{2P'(s)},\quad(9)$$

where P', Q' are time differential operators and S_{ij}, e_{ij} are the deviatoric components of the stress and strain tensors. Thus, eqs. (5)–(8) can accordingly be expressed as

$$\tilde{J}_1(s)=\frac{2P'(s)\left[6KP'(s)+7Q'(s)\right]}{sQ'(s)\left[3KP'(s)+2Q'(s)\right]},\quad(10)$$

$$\tilde{J}_2(s)=\frac{2P'(s)\left[6KP'(s)+Q'(s)\right]}{sQ'(s)\left[3KP'(s)+2Q'(s)\right]},\quad(11)$$

$$\tilde{J}_3(s)=\frac{6KP'(s)+7Q'(s)}{s\left[3KP'(s)+2Q'(s)\right]},\quad(12)$$

$$\tilde{J}_4(s)=\frac{6KP'(s)+Q'(s)}{s\left[3KP'(s)+2Q'(s)\right]},\quad(13)$$

To solve eq. (1) with respect to time t, we choose the trapezoidal rule for discretization, and obtain

$$C_{ij}(\boldsymbol{x})u_j(\boldsymbol{x},mh)=\int_S\Bigg[U_{ij}(\boldsymbol{x},\boldsymbol{y},0)p_j(\boldsymbol{y},mh)+\frac{h}{2}p_j(\boldsymbol{y},mh)\hat{U}_{ij}(\boldsymbol{x},\boldsymbol{y},0)\Bigg]\mathrm{d}S(\boldsymbol{y})-\int_S\Bigg[P_{ij}(\boldsymbol{x},\boldsymbol{y},0)u_j(\boldsymbol{y},mh)+\frac{h}{2}u_j(\boldsymbol{y},mh)\hat{P}_{ij}(\boldsymbol{x},\boldsymbol{y},0)\Bigg]\mathrm{d}S(\boldsymbol{y})+R_i^*[(m-1)h],\quad(14)$$

where $t=mh$ means the time t is divided into m intervals of equal duration h, $\hat{U}_{ij}(\boldsymbol{x},\boldsymbol{y},\boldsymbol{t})=\partial U_{ij}(\boldsymbol{x},\boldsymbol{y},\boldsymbol{t})/\partial t$ and $\hat{P}_{ij}(\boldsymbol{x},\boldsymbol{y},\boldsymbol{t})=\partial P_{ij}(\boldsymbol{x},\boldsymbol{y},\boldsymbol{t})/\partial t$. $R_i^*[(m-1)h]$ is the entire history for $t<mh$, and is given by

$$R_i^*[(m-1)h]=\frac{h}{2}\int_S\hat{U}_{ij}(\boldsymbol{x},\boldsymbol{y},h)p_j(\boldsymbol{y},0)\mathrm{d}S(\boldsymbol{y})-\frac{h}{2}\int_S\hat{P}_{ij}(\boldsymbol{x},\boldsymbol{y},h)u_j(\boldsymbol{y},0)\mathrm{d}S(\boldsymbol{y})\ (m=1),$$

$$R_i^*[(m-1)h]=h\int_S\sum_{q=1}^{m-1}\hat{U}_{ij}(\boldsymbol{x},\boldsymbol{y},qh)p_j\left(\boldsymbol{y},[n-q]h\right)\mathrm{d}S(\boldsymbol{y})-h\int_S\sum_{q=1}^{m-1}\hat{P}_{ij}(\boldsymbol{x},\boldsymbol{y},qh)u_j\left(\boldsymbol{y},[n-q]h\right)\mathrm{d}S(\boldsymbol{y})+\frac{h}{2}\int_S\hat{U}_{ij}(\boldsymbol{x},\boldsymbol{y},h)p_j(\boldsymbol{y},0)\mathrm{d}S(\boldsymbol{y})-\frac{h}{2}\int_S\hat{P}_{ij}(\boldsymbol{x},\boldsymbol{y},h)u_j(\boldsymbol{y},0)\mathrm{d}S(\boldsymbol{y})\ (m=2,3\ldots N).\quad(15)$$

Similar to the 2D FMBEM for elasticity problem, we can also easily establish the multipole expansion formulations based on eq. (14). If we employ the constant boundary elements, the integrals in eq. (14), such as $\int_S U_{ij}(\boldsymbol{x},\boldsymbol{y},\tau)p_j(\boldsymbol{y},t)\mathrm{d}S(\boldsymbol{y})$ and $\int_S P_{ij}(\boldsymbol{x},\boldsymbol{y},\tau)u_j(\boldsymbol{y},t)\mathrm{d}S(\boldsymbol{y})$ can be written in a complex form based on eqs. (2) and (3):

$$\begin{aligned}D_p(z_0,t,\tau)&=\int_S U_{ij}(\boldsymbol{x},\boldsymbol{y},\tau)p_j(\boldsymbol{y},t)\mathrm{d}S(\boldsymbol{y})\\&=\frac{1}{16\pi}\int_S\Big\{J_1(\tau)Ge(z_0,z)\,p(z,t)-J_2(\tau)z_0\overline{Ge'(z_0,z)\,p(z,t)}\\&+J_2(\tau)z\overline{Ge'(z_0,z)\,p(z,t)}+J_1(\tau)\overline{Ge(z_0,z)}p(z,t)\Big\}\mathrm{d}S(z),\end{aligned}\tag{16}$$

$$\begin{aligned}D_u(z_0,t,\tau)&=\int_S P_{ij}(\boldsymbol{x},\boldsymbol{y},\tau)u_j(\boldsymbol{y},t)\mathrm{d}S(\boldsymbol{y})\\&=-\frac{1}{8\pi}\int_S\Big\{J_3(\tau)Ge'(z_0,z)n(z)u(z,t)\\&-J_4(\tau)z_0\overline{Ge''(z_0,z)n(z)u(z,t)}\\&+J_4(\tau)z\overline{Ge''(z_0,z)n(z)u(z,t)}+J_4(\tau)\overline{Ge'(z_0,z)}\\&\times\Big[n(z)\overline{u(z,t)}+\overline{n(z)}u(z,t)\Big]\Big\}\mathrm{d}S(z),\end{aligned}\tag{17}$$

where $Ge(z_0,z)=-\ln(z_0-z)$, $z=y_1+iy_2$ is the field point, and $z_0=x_1+ix_2$ is the collection point. $u(z)=u_1+iu_2$, $p(z)=p_1+ip_2$ and $n(z)=n_1+in_2$ are the complex displacement, traction and normal at z, respectively.

By means of the multipole expansions developed in ref. [24], we can further rewrite eqs. (16) and (17) as follows:

$$\begin{aligned}D_p(z_0,t,\tau)=\frac{1}{16\pi}\Bigg[&\sum_{k=0}^{\infty}O_k(z_0-z_c)R_k(z_c,t,\tau)\\&+z_0\sum_{k=0}^{\infty}\overline{O_{k+1}(z_0-z_c)A_k(z_c,t,\tau)}\\&+\sum_{k=0}^{\infty}\overline{O_k(z_0-z_c)}W_k(z_c,t,\tau)\Bigg],\end{aligned}\tag{18}$$

$$\begin{aligned}D_u(z_0,t,\tau)=\frac{1}{8\pi}\Bigg[&\sum_{k=1}^{\infty}O_k(z_0-z_c)Y_k(z_c,t,\tau)\\&+z_0\sum_{k=0}^{\infty}\overline{O_{k+1}(z_0-z_c)B_k(z_c,t,\tau)}\\&+\sum_{k=0}^{\infty}\overline{O_k(z_0-z_c)}V_k(z_c,t,\tau)\Bigg],\end{aligned}\tag{19}$$

where R_k, A_k, W_k, Y_k, B_k, and V_k are called moments about z_c which are independent of the collocation point z_0 and only need to be computed once; they are given by

$$R_k(z_c,t,\tau)=J_1(\tau)\int_S I_k(z-z_c)p(z,t)\mathrm{d}S(z)\quad(k\geqslant 0),\tag{20}$$

$$A_k(z_c,t,\tau)=J_2(\tau)\int_S I_k(z-z_c)p(z,t)\mathrm{d}S(z)\quad(k\geqslant 0),\tag{21}$$

$$\begin{aligned}W_k(z_c,t,\tau)=&J_1(\tau)\int_S\overline{I_k(z-z_c)}p(z,t)\mathrm{d}S(z)\\&-J_2(\tau)\int_S\overline{I_{k-1}(z-z_c)}z\overline{p(z,t)}\mathrm{d}S(z)\ (k\geqslant 1),\end{aligned}\tag{22}$$

$$W_0(z_c,t,\tau)=J_1(\tau)\int_S p(z,t)\mathrm{d}S(z),\tag{23}$$

$$Y_k(z_c,t,\tau)=J_3(\tau)\int_S I_{k-1}(z-z_c)n(z)u(z,t)\mathrm{d}S(z)\ (k\geqslant 1),\tag{24}$$

$$B_k(z_c,t,\tau)=J_4(\tau)\int_S I_{k-1}(z-z_c)n(z)u(z,t)\mathrm{d}S(z),\tag{25}$$

$$\begin{aligned}V_k(z_c,t,\tau)=&\int_S J_4(\tau)\Big\{\overline{I_{k-1}(z-z_c)}[n(z)\overline{u(z,t)}+\overline{n(z)}u(z,t)]\\&-\overline{I_{k-2}(z-z_c)}z\overline{n(z)u(z,t)}\Big\}\mathrm{d}S(z)\quad(k\geqslant 2),\end{aligned}\tag{26}$$

$$V_1(z_c,t,\tau)=J_4(\tau)\int_S[n(z)\overline{u(z,t)}+\overline{n(z)}u(z,t)]\mathrm{d}S(z),\tag{27}$$

and O_k and I_k are two auxiliary functions:

$$I_k=\frac{z^k}{k!}\quad\text{for}\quad k\geqslant 0,\tag{28}$$

$$O_0(z)=-\ln(z),\quad O_k(z)=\frac{(k-1)!}{z^k}\quad\text{for}\quad k\geqslant 1.\tag{29}$$

Up to now, the fast multipole BEM formulations for 2D viscoelasticity have been obtained. Since the M2M, M2L and L2L translations remain the same as those for the elastostatic problems, it is not difficult to program the present 2D viscoelastic counterpart based on the fast multipole BEM code for 2D elastic problems. Detailed analysis and formulations of the subsequent multipole translations and implementations of FMM can be found in ref. [24].

3 FMBEM modeling of multi-inclusion composites with interfacial imperfection

Consider a 2D viscoelastic domain V_0 containing N elastic inclusions V_α. The conventional boundary integral equation (BIE) for the matrix domain V_0 can be written as eq. (1), while each inclusion domain can be written as

$$\begin{aligned}C_{ij}(\boldsymbol{x})u_j^\alpha(\boldsymbol{x},t)=&\int_{S_\alpha}[U_{ij}^\alpha(\boldsymbol{x},\boldsymbol{y})p_j^\alpha(\boldsymbol{y},t)-P_{ij}^\alpha(\boldsymbol{x},\boldsymbol{y})u_j^\alpha(\boldsymbol{y},t)]\mathrm{d}S(\boldsymbol{y}),\\&(\alpha=1,2,...,N),\quad\forall x\in S_\alpha,\end{aligned}\tag{30}$$

where S_α is the boundary of the αth inclusion.

After discretization with the boundary elements, eqs. (1) and (30) can be written in a matrix form for the αth inclusion as follows:

$$\begin{bmatrix} \boldsymbol{A}_{11}^{0\prime} & \boldsymbol{A}_{12}^{0\prime} & \boldsymbol{A}_{13}^{\alpha\prime} \\ \boldsymbol{A}_{21}^{0\prime} & \boldsymbol{A}_{22}^{0\prime} & \boldsymbol{A}_{23}^{\alpha\prime} \\ \boldsymbol{A}_{31}^{0\prime} & \boldsymbol{A}_{32}^{0\prime} & \boldsymbol{A}_{33}^{\alpha\prime} \end{bmatrix} \begin{Bmatrix} \boldsymbol{U}_t^0 \\ \boldsymbol{P}_t^0 \\ \boldsymbol{U}_t^{\alpha 0} \end{Bmatrix} = \begin{bmatrix} \boldsymbol{B}_{11}^{0\prime} & \boldsymbol{B}_{12}^{0\prime} & \boldsymbol{B}_{13}^{\alpha\prime} \\ \boldsymbol{B}_{21}^{0\prime} & \mathbf{B}_{22}^{0\prime} & \boldsymbol{B}_{23}^{\alpha\prime} \\ \boldsymbol{B}_{31}^{0\prime} & \boldsymbol{B}_{32}^{0\prime} & \boldsymbol{B}_{33}^{\alpha\prime} \end{bmatrix} \begin{Bmatrix} \overline{\boldsymbol{U}}_t^0 \\ \overline{\boldsymbol{P}}_t^0 \\ \boldsymbol{P}_t^{\alpha 0} \end{Bmatrix} + \left\{ \boldsymbol{R}_m^{\prime *} \right\}, \quad (31)$$

$$\boldsymbol{G}^{\alpha} \boldsymbol{P}^{\alpha\alpha}(t) = \boldsymbol{H}^{\alpha} \boldsymbol{U}^{\alpha\alpha}(t), \quad (32)$$

where $\boldsymbol{U}_t^0$ and $\boldsymbol{P}_t^0$ are the unknown nodal displacement and traction vectors at time t respectively, while $\overline{\boldsymbol{U}}_t^0$ and $\overline{\boldsymbol{P}}_t^0$ are the given nodal displacement and traction vectors at time t respectively; $\boldsymbol{U}_t^{\alpha 0}$ is the displacement vector of the matrix at the boundary, and $\boldsymbol{P}_t^{\alpha 0}$ is the traction vector exerted by the inclusion on the matrix; $\boldsymbol{U}^{\alpha\alpha}(t)$ is the displacement vector of the inclusion at the interface at time t, while $\boldsymbol{P}^{\alpha\alpha}(t)$ is the traction vector exerted by the matrix on the inclusion at time t. $\boldsymbol{R}_m^{\prime *}$ is the entire history which can be obtained from earlier time steps by the matrix.

For an imperfect interface, we use a Kelvin type viscoelastic interface, in which a linear spring and a linear dashpot are connected in parallel. It can be written in the following mathematical form:

$$\sigma_r^m = \sigma_r^f = k_{0r} \Delta u_r + k_{1r} \frac{\partial \Delta u_r}{\partial t}. \quad (33)$$

$$\tau_{r\theta}^m = \tau_{r\theta}^f = k_{0\theta} \Delta u_\theta + k_{1\theta} \frac{\partial \Delta u_\theta}{\partial t}, \quad (34)$$

where Δu_r and Δu_θ are the relative sliding displacements between the matrix and inclusions, $\partial \Delta u_r / \partial t$ and $\partial \Delta u_\theta / \partial t$ are the sliding velocity. k_{0r}, $k_{0\theta}$ and k_{1r}, $k_{1\theta}$ are the elastic constants and viscous coefficients of the viscoelastic interface, respectively. Therefore, we can get the boundary conditions in the following matrix form:

$$\boldsymbol{U}^{\alpha 0}(t) - \boldsymbol{U}^{\alpha\alpha}(t) = \boldsymbol{k}^{\alpha}(t) * \boldsymbol{P}^{\alpha 0}(t) \quad (35)$$

$$\boldsymbol{P}^{\alpha 0}(t) = -\boldsymbol{P}^{\alpha\alpha}(t), \quad (36)$$

where * represents the convolution, $\boldsymbol{k}^{\alpha}(t)$ is called the flexibility matrix which is diagonal, and can be described in the Laplace domain as follows:

$$\tilde{\boldsymbol{k}}^{\alpha} = -\boldsymbol{Q}_{\alpha}^{-1} \begin{bmatrix} 1/(k_{0r} + k_{1r} s) & 0 \\ 0 & 1/(k_{0\theta} + k_{1\theta} s) \end{bmatrix} \boldsymbol{Q}_{\alpha}, \quad (37)$$

in which $\boldsymbol{Q}_{\alpha}$ is the coordinate transformation matrix to translate the nodal values from the αth local element coordinate system to the global coordinate system. To avoid an unrealistic radial overlap of the two materials at the interface, when $\sigma_r^m = \sigma_r^f < 0$, let

$$\tilde{\boldsymbol{k}}^{\alpha} = -\boldsymbol{Q}_{\alpha}^{-1} \begin{bmatrix} 0 & 0 \\ 0 & 1/(k_{0\theta} + k_{1\theta} s) \end{bmatrix} \boldsymbol{Q}_{\alpha}. \quad (38)$$

Simialr to eq. (14), we can also discretize eq. (35) by the trapezoidal rule. Therefore, according to eqs. (35) and (36), eqs. (31) and (32) can be rewritten in the time domain as follows:

$$\begin{bmatrix} \boldsymbol{A}_{11}^{0\prime} & \boldsymbol{A}_{12}^{0\prime} & \boldsymbol{A}_{13}^{\alpha\prime} & -\boldsymbol{B}_{13}^{\alpha\prime} \\ \boldsymbol{A}_{21}^{0\prime} & \boldsymbol{A}_{22}^{0\prime} & \boldsymbol{A}_{23}^{\alpha\prime} & -\boldsymbol{B}_{23}^{\alpha\prime} \\ \boldsymbol{A}_{31}^{0\prime} & \boldsymbol{A}_{32}^{0\prime} & \boldsymbol{A}_{33}^{\alpha\prime} & -\boldsymbol{B}_{33}^{\alpha\prime} \\ \mathbf{0} & \mathbf{0} & \boldsymbol{H}_{\alpha} & \mathbf{G}_{\alpha} - \boldsymbol{H}^{\prime}{}_{\alpha} \boldsymbol{k}_{\alpha}^{\prime} \end{bmatrix} \begin{Bmatrix} \boldsymbol{U}_t^0 \\ \boldsymbol{P}_t^0 \\ \boldsymbol{U}_t^{\alpha 0} \\ \boldsymbol{P}_t^{\alpha 0} \end{Bmatrix} = \begin{bmatrix} \boldsymbol{B}_{11}^{0\prime} & \boldsymbol{B}_{12}^{0\prime} \\ \boldsymbol{B}_{21}^{0\prime} & \boldsymbol{B}_{22}^{0\prime} \\ \boldsymbol{B}_{31}^{0\prime} & \boldsymbol{B}_{32}^{0\prime} \\ \mathbf{0} & \mathbf{0} \end{bmatrix} \begin{Bmatrix} \overline{\boldsymbol{U}}_t^0 \\ \overline{\boldsymbol{P}}_t^0 \end{Bmatrix} + \begin{Bmatrix} \boldsymbol{R}_m^{\prime *} \\ \boldsymbol{R}_f^{\prime \alpha *} \end{Bmatrix}, \quad (39)$$

where $\boldsymbol{k}_{\alpha}^{\prime} = (h/2)\boldsymbol{k}^{\alpha}(0)$ and $\boldsymbol{R}_f^{\prime \alpha *}$ is the entire history from earlier time steps by the αth inclusion. The final equation system for the 2D viscoelastic solid with multiple elastic inclusions, which involves the effect of viscoelastic imperfect interfaces, can be obtained as

$$\begin{bmatrix} \boldsymbol{A}_{11}^{0\prime} & \boldsymbol{A}_{12}^{0\prime} & \boldsymbol{A}_{13}^{1\prime} & \cdots & \boldsymbol{A}_{13}^{n\prime} & -\boldsymbol{B}_{13}^{1\prime} & \cdots & -\boldsymbol{B}_{13}^{n\prime} \\ \boldsymbol{A}_{21}^{0\prime} & \boldsymbol{A}_{22}^{0\prime} & \boldsymbol{A}_{23}^{1\prime} & \cdots & \boldsymbol{A}_{23}^{n\prime} & -\boldsymbol{B}_{23}^{1\prime} & \cdots & -\boldsymbol{B}_{23}^{n\prime} \\ \boldsymbol{A}_{31}^{1\prime} & \boldsymbol{A}_{32}^{1\prime} & \boldsymbol{A}_{33}^{11\prime} & \cdots & \boldsymbol{A}_{33}^{1n\prime} & -\boldsymbol{B}_{33}^{11\prime} & \cdots & -\boldsymbol{B}_{33}^{1n\prime} \\ \vdots & \vdots & \vdots & \ddots & \vdots & \vdots & \ddots & \vdots \\ \boldsymbol{A}_{31}^{n\prime} & \boldsymbol{A}_{32}^{n\prime} & \boldsymbol{A}_{33}^{n1\prime} & \cdots & \boldsymbol{A}_{33}^{nn\prime} & -\boldsymbol{B}_{33}^{n1\prime} & \cdots & -\boldsymbol{B}_{33}^{nn\prime} \\ \mathbf{0} & \mathbf{0} & \boldsymbol{H}_1 & \cdots & \mathbf{0} & \boldsymbol{G}_1 - \boldsymbol{H}_1^{\prime} \boldsymbol{k}_1^{\prime} & \cdots & \mathbf{0} \\ \vdots & \vdots & \vdots & \ddots & \vdots & \vdots & \ddots & \vdots \\ \mathbf{0} & \mathbf{0} & \mathbf{0} & \cdots & \boldsymbol{H}_n & \mathbf{0} & \cdots & \boldsymbol{G}_n - \boldsymbol{H}_n^{\prime} \boldsymbol{k}_n^{\prime} \end{bmatrix} \begin{Bmatrix} \boldsymbol{U}_t^0 \\ \boldsymbol{P}_t^0 \\ \boldsymbol{U}_t^{10} \\ \vdots \\ \boldsymbol{U}_t^{n0} \\ \boldsymbol{P}_t^{10} \\ \vdots \\ \boldsymbol{P}_t^{n0} \end{Bmatrix}$$

$$= \begin{bmatrix} \boldsymbol{B}_{11}^{0\prime} & \boldsymbol{B}_{12}^{0\prime} \\ \boldsymbol{B}_{21}^{0\prime} & \boldsymbol{B}_{22}^{0\prime} \\ \boldsymbol{B}_{31}^{1\prime} & \boldsymbol{B}_{32}^{1\prime} \\ \vdots & \vdots \\ \boldsymbol{B}_{31}^{n\prime} & \boldsymbol{B}_{32}^{n\prime} \\ \mathbf{0} & \mathbf{0} \\ \mathbf{0} & \mathbf{0} \\ \mathbf{0} & \mathbf{0} \end{bmatrix} \begin{Bmatrix} \overline{\boldsymbol{U}}_t^0 \\ \overline{\boldsymbol{P}}_t^0 \end{Bmatrix} + \begin{Bmatrix} \boldsymbol{R}_m^{\prime *} \\ \boldsymbol{R}_f^{\prime *} \end{Bmatrix}. \quad (40)$$

Preconditioner is a crucial part to ensure the efficiency and accuracy of the fast multipole BEM. The preconditioner used here for eq. (40) is a block diagonal preconditioner proposed by Liu [26]. In the matrix domain, a diagonal sub-matrix is formed on each leaf by direct evaluations of the kernels within that leaf, while in the inclusions domain, the sub-matrix $\boldsymbol{G}_i - \boldsymbol{H}_i^{\prime} \boldsymbol{k}_i^{\prime}$ along the main diagonal is used for each inclusion. However, it should be mentioned that in the implementation of such a model by numerical method

presented above, a numerical trial should be made. First, calculation based on the interface condition in eq. (37) is implemented, and then the sign of normal stress at all nodal points along the interface is checked. The interface condition should be corrected to eq. (38) at those nodal points where compressive normal stresses appear. The calculation then proceeds in such an iterative way. The calculation will not be ended until at any nodal point the same interface condition, either eq. (37) or eq. (38), is satisfied.

4 Numerical examples

Several examples are considered here to verify the proposed numerical procedures of the fast multipole BEM for 2D multi-domain viscoelastic problems with interfacial bonding imperfection. Analytical solutions are also developed here to compare with the numerical results. In this paper, two commonly used models are represented to simulate the linear viscoelastic behavior of the real materials. Figure 1(a) shows the Burgers model (Type 1) which describes a body that has instantaneous elasticity, delayed elasticity and viscous flow. It can also be used to simulate the materials working under high stress or at high temperature. Figure 1(b) presents the two Voigt+one spring model (Type 2) which is commonly used, because it can fit experimental curves better. Thus, we often use it to describe the viscoelastic solids in engineering, such as asphalt concrete and rock. The operators $P'(s)$, $Q'(s)$ for these two types can be written as

$$\begin{aligned} P'(s) &= 1+\left(\frac{\eta_1}{E_1}+\frac{\eta_1+\eta_2}{E_2}\right)s+\frac{\eta_1\eta_2}{E_1E_2}s^2, \\ Q'(s) &= \eta_1 s+\frac{\eta_1\eta_2}{E_2}s^2 \end{aligned} \tag{41}$$

for Type 1, and

$$\begin{aligned} P'(s) &= 1+\frac{E_1\eta_2+E_2\eta_1+E_0\eta_1+E_0\eta_2}{E_1E_2+E_1E_0+E_0E_2}s \\ &\quad +\frac{\eta_1\eta_2}{E_1E_2+E_1E_0+E_0E_2}s^2, \\ Q'(s) &= \frac{E_0E_1E_2}{E_1E_2+E_1E_0+E_0E_2}+\frac{E_0E_1\eta_2+E_0E_2\eta_1}{E_1E_2+E_1E_0+E_0E_2}s \\ &\quad +\frac{E_0\eta_1\eta_2}{E_1E_2+E_1E_0+E_0E_2}s^2 \end{aligned} \tag{42}$$

for Type 2.

4.1 Analytical solution for concentric cylinder model

We first study a concentric cylinder model (Figure 2) to verify the BEM programme for multi-domain problems with imperfect viscoelastic interface. In this case, a solid

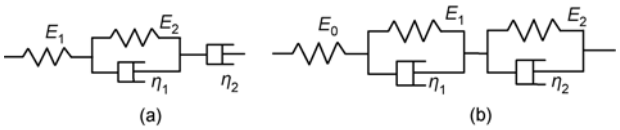

Figure 1 Two models representing the linear viscoelastic behavior.

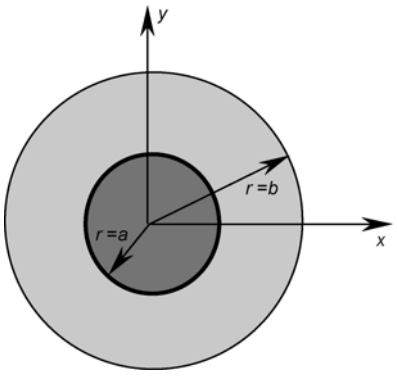

Figure 2 Concentric cylindrical model.

cylinder inclusion is embedded in a larger cylinder matrix, where the matrix is isotropic and linear viscoelastic (of Type 1), and the inclusion is isotropic elastic. Applying the theory of elasticity for plane strain case in the polar coordinate system, one can derive the following expressions for the radial displacements and stress fields in the inclusion and matrix, respectively

$$u_r^f = A_f r,\ 0 \leqslant r \leqslant a, \tag{43}$$

$$u_r^m = A_m r+\frac{B_m}{r},\ a \leqslant r \leqslant b, \tag{44}$$

$$\sigma_r^f = \frac{A_f E_f}{(1+\nu_f)(1-2\nu_f)},\ 0 \leqslant r \leqslant a, \tag{45}$$

$$\sigma_r^m = \frac{E_m}{(1+\nu_m)(1-2\nu_m)}\left(A_m-\frac{B_m}{r^2}+2\nu_m\frac{B_m}{r^2}\right),\ a \leqslant r \leqslant b. \tag{46}$$

To reflect the interface imperfections, eq. (33) is introduced. Besides, a radial displacement δ or a radial tension δ is prescribed on the outer boundary of the matrix $r=b$ here. Thus the boundary and interface conditions are

$$r=b:\ u_r^m=\delta \ \text{(condition 1) or}\ \sigma_r^m=\delta\ \text{(condition 2)}, \tag{47}$$

$$r=a:\ \sigma_r^m=\sigma_r^f=k_{0r}\Delta u_r+k_{1r}\frac{\partial \Delta u_r}{\partial t}. \tag{48}$$

Effective elastic material properties can be directly converted to viscoelastic properties using the correspondence principle on the basis of Laplace transform. The correspondence process is performed by replacing each elastic modulus with the corresponding modulus related to time. It should be mentioned that the elastic modulus of the inclu-

sion and the bulk modulus of each phase are assumed constant. Therefore, three constants A_f, A_m and B_m can be solved by combining eqs. (43)–(48) in the Laplace domain,

$$\tilde{A}_m = \frac{\delta b\left(1+\tilde{T}^2-2\tilde{\nu}_m\right)}{s\left(a^2+b^2-\tilde{T}a^2+\tilde{T}b^2-2b^2\tilde{\nu}_m\right)},$$
$$\tilde{A}_f = \frac{2\tilde{T}b^2\delta\left(1-\tilde{\nu}_m\right)}{\tilde{\alpha}s\left(a^2+b^2-\tilde{T}a^2+\tilde{T}b^2-2b^2\tilde{\nu}_m\right)}, \quad (49)$$
$$\tilde{B}_m = \frac{a^2b^2\delta\left(1-\tilde{T}\right)}{s\left(a^2+b^2-\tilde{T}a^2+\tilde{T}b^2-2b^2\tilde{\nu}_m\right)}$$

for condition 1, and

$$\tilde{A}_m = \frac{\tilde{\beta}\delta b^2\left(2\tilde{\nu}_m-1-\tilde{T}\right)}{s\left(a^2-b^2+2b^2\tilde{\nu}_m-2a^2\tilde{\nu}_m-\tilde{T}a^2-\tilde{T}b^2+2\tilde{T}a^2\tilde{\nu}_m\right)},$$
$$\tilde{A}_f = \frac{2\tilde{T}\tilde{\beta}\delta b^2\left(\tilde{\nu}_m-1\right)}{\tilde{\alpha}s\left(a^2-b^2+2b^2\tilde{\nu}_m-2a^2\tilde{\nu}_m-\tilde{T}a^2-\tilde{T}b^2+2\tilde{T}a^2\tilde{\nu}_m\right)},$$
$$\tilde{B}_m = \frac{\tilde{\beta}\delta a^2b^2\left(\tilde{T}-1\right)}{s\left(a^2-b^2+2b^2\tilde{\nu}_m-2a^2\tilde{\nu}_m-\tilde{T}a^2-\tilde{T}b^2+2\tilde{T}a^2\tilde{\nu}_m\right)} \quad (50)$$

for con`dition 2, and

$$\tilde{T} = \frac{a\tilde{\alpha}\tilde{\beta}\left(k_{0r}+k_{1r}s\right)}{\tilde{\alpha}+a\tilde{\beta}\left(k_{0r}+k_{1r}s\right)}, \quad \tilde{\alpha} = \frac{E_f(1+\tilde{\nu}_m)\left(1-2\tilde{\nu}_m\right)}{\tilde{E}_m(1+\nu_f)\left(1-2\nu_f\right)},$$
$$\tilde{\beta} = \frac{(1+\tilde{\nu}_m)\left(1-2\tilde{\nu}_m\right)}{\tilde{E}_m}, \quad (51)$$

$$\tilde{E}_m = \frac{9\tilde{G}_mK_m}{\left(3K_m+\tilde{G}_m\right)}, \quad \tilde{\nu}_m = \frac{3K_m-2\tilde{G}_m}{2\left(3K_m+\tilde{G}_m\right)}, \tilde{G}_m = \frac{Q'(s)}{2P'(s)}. \quad (52)$$

For example, the radial displacements of the inclusion in the Laplace image space at $r=a$ under condition 1 can be written as

$$\tilde{u}_{ra}^f(t) = \frac{2\tilde{T}ab^2\delta\left(1-\tilde{\nu}_m\right)}{\tilde{\alpha}s\left(a^2+b^2-\tilde{T}a^2+\tilde{T}b^2-2b^2\tilde{\nu}_m\right)}. \quad (53)$$

The following material parameters for the matrix are used in numerical and analytical calculation:

$$E_1 = 10 \text{ MPa}, \ E_2 = 25 \text{ MPa},$$
$$\eta_1 = 750 \text{ MPa}, \ \eta_2 = 35 \text{ MPa}\cdot\text{s}. \quad (54)$$

Three different values of Young's modulus of the inclusion E_f=1 MPa, 10 MPa and 100 MPa (Figures 3 and 4), and five different values of the interface parameters $k_{0r}=k_{1r}=k$=0.1, 1, 10, 100 and 10^8 (Figure 5) have been considered. The results calculated by the fast multipole BEM are compared with the exact analytical solution presented above. It is shown that the FMBEM results are in excellent agreement with the analytical solutions, which indicates that the developed fast multipole BEM is adequate to predict the viscoelastic behavior of multi-inclusion composites with imperfect viscoelastic interfaces.

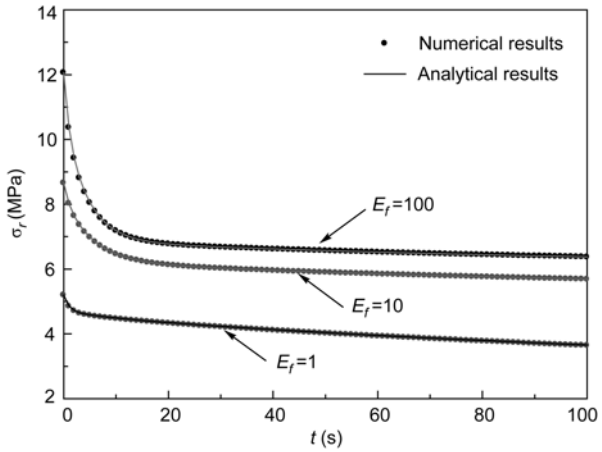

Figure 3 Comparison between analytical and numerical results of stresses at $r=b$ for different values of E_f(MPa) (condition 1, k_{0r}=10 MPa/m, k_{1r}=100 MPa/m).

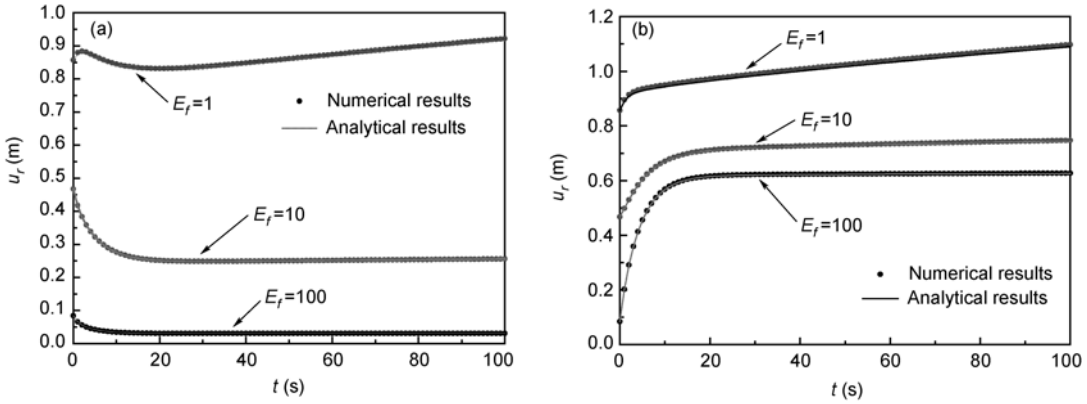

Figure 4 Comparison between analytical and numerical results for different values of E_f. (MPa). (a) Displacement of inclusion; (b) displacement of matrix, both at $r=a$ (condition 1, k_{0r}=10 MPa/m, k_{1r}=100 MPa/m).

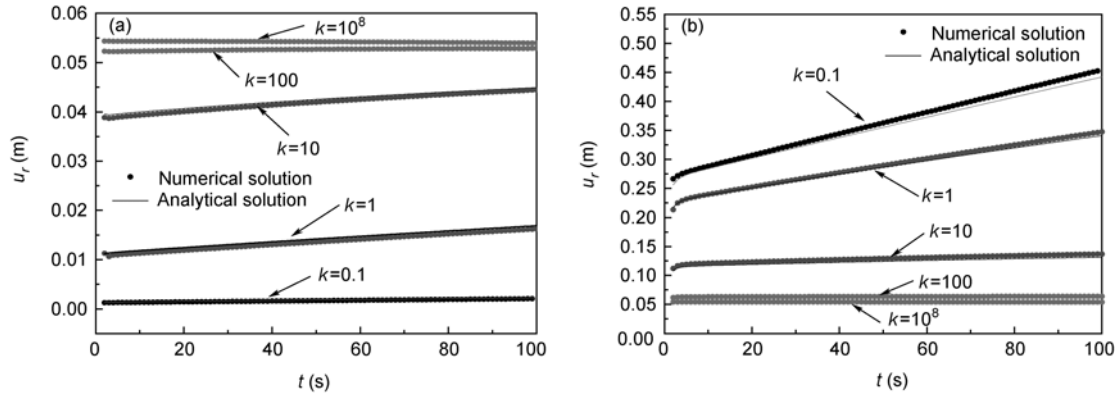

Figure 5 Comparison between analytical and numerical results for different values of k (MPa/m). (a) Displacement of inclusion; (b) displacement of matrix, both at $r=a$ (condition 2, E_f=10 MPa).

4.2 Multi-inclusion problems

We next study the properties of multi-phase planar viscoelastic composites subjected to plane strain assumption. The model examined is that of randomly distributed circular elastic inclusions embedded in a matrix possessing linear viscoelastic property, which is modeled by Burgers type model. First, we establish a micromechanical method, based on the Mori-Tanaka method, for determining effective composite properties when the matrix is viscoelastic with imperfect viscoelastic interface. Due to the isotropy of the overall stiffness tensor, the effective shear modulus G and planer bulk modulus K for the composite with circle inclusions, estimated by Mori-Tanaka method, are expressed in the Laplace domain as follows:

$$\tilde{G}=\tilde{G}_0\left[1+\frac{2f}{(1-f)\left(K_0+2\tilde{G}_0\right)/\left(K_0+\tilde{G}_0\right)+2\tilde{G}_0/\left(\tilde{G}_1'-\tilde{G}_0\right)}\right], \tag{55}$$

$$\tilde{K}=K_0\left[1+\frac{f}{(1-f)K_0/\left(K_0+\tilde{G}_0\right)+K_0/\left(\tilde{K}_1'-K_0\right)}\right], \tag{56}$$

$$\tilde{G}_0=\frac{Q'(s)}{2P'(s)},$$

where K_0 and $\tilde{G}_0$ are the bulk modulus and viscoelastic shear modulus for the matrix, f is the volume content of the inclusions, and $\tilde{K}_1'$, $\tilde{G}_1'$ are the effective bulk modulus and effective shear modulus for the inclusion, respectively, in which the interface effect has already been taken into account. In the computations, the following interface constants are taken equal in magnitude

$$k_{0r}=k_{0\theta}=k_0,\ k_{1r}=k_{1\theta}=k_1. \tag{57}$$

According to the equivalent method idea proposed by Achenbach and Zhu [31], we can further get the effective shear modulus and effective bulk modulus for the inclusions with viscoelastic interface in the image domain. It can be obtained as follows:

$$\tilde{G}_1'=\frac{aG_f\left(k_0+k_1s\right)}{a\left(k_0+k_1s\right)+2G_f}, \tag{58}$$

$$\tilde{K}_1'=\frac{aG_f\left(k_0+k_1s\right)\left[a\left(k_0+k_1s\right)\left(1+\nu_f\right)+2G_f\right]}{\left[a\left(k_0+k_1s\right)+2G_f\right]\left[a\left(k_0+k_1s\right)\left(1-\nu_f\right)+2G_f\right]}. \tag{59}$$

Based on the relationship between the elastic constants, the effective Young's modulus of the composite can be obtained quite easily for the two-dimensional cases in the Laplace domain:

$$\tilde{E}=\frac{4\tilde{G}\tilde{K}}{\tilde{K}+\tilde{G}}. \tag{60}$$

Using the same method and hypothesis as Example 1 discussed, the constitutive equation of the composite in the Laplace image domain becomes

$$\varepsilon(s)=\frac{\overline{\sigma}}{s\tilde{E}}, \tag{61}$$

where $\overline{\sigma}$ is the uniaxial tension acting on the opposite edges, $\varepsilon(s)$ is the average strain of the composite along the tensile direction in the image domain.

By Laplace integral inverse transform, one can obtain from eq. (61) the time variation of the average strain of the composite along the tensile direction.

For the multi-inclusion model, analytical solutions are obtained for the average strain, which can be employed to compare with the developed FMBEM results. For calculating the average strain along the tensile direction, we consider a square domain subjected to a uniform unit uniaxial tension in x-direction, see Figure 6. It has been reported by Hu et al. [32] that the results tend to be stable when the number of inclusions is greater than 100, and the body presents apparent homogeneous and isotropic characteristic. Therefore, in our models, the number of inclusions is kept

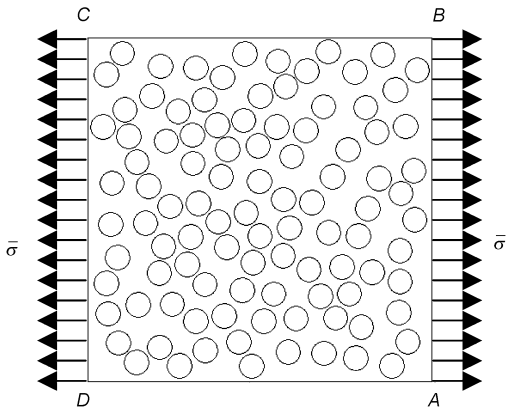

Figure 6 Viscoelastic composite containing multiple elastic circular inclusions.

to be 100, and the radius of inclusions is changed with the volume content of the inclusion. Once all fast multipole boundary functions are determined, one can use the results to estimate the average strain of materials with multi-inclusions. The average strain in the transverse direction is determined by

$$\bar{\varepsilon}_x = \frac{\bar{U}_{AB} + \bar{U}_{CD}}{L}, \tag{62}$$

where L is the length of the square sheet, and $\bar{U}$ is the effective displacement calculated from the fast multipole BEM results, and it can be written as

$$\bar{U} = \frac{\sum_e^n \int_{\Gamma_e} U_e d\Gamma_e}{L}, \tag{63}$$

where U_e is the displacement of the element. In civil engineering, creep problems often occur in many cases, such as pressure pipes and asphalt pavement. It is known that most engineering materials more or less have the viscoelastic characteristic and this property will make many structures suffer from creep problems under some environmental conditions. Here, we also investigate the creep problem of the multi-inclusion composite from the numerical results:

$$J(t) = \frac{\bar{\varepsilon}_x}{\bar{\sigma}}, \tag{64}$$

where $J(t)$ is the creep compliance, which is defined as the strain function in time resulting from the application of a unit step stress. In linearly viscoelastic materials, the creep compliance is independent of the stress level.

The analytical and numerical results for the average strain of the multi-inclusion composite are calculated for the following Burgers model parameters for the matrix:

$$\begin{aligned} &E_1 = 2.328 \text{ MPa}, \ E_2 = 1.389 \text{ MPa}, \\ &\eta_1 = 752.516 \text{ MPa}, \ \eta_2 = 31.549 \text{ MPa}\cdot\text{s}. \end{aligned} \tag{65}$$

The numerical solution is obtained by using 200 elements on the outer boundary and 20 elements on each interface of the inclusions. When k_0=k_1=10, the increase of the interface parameters has little effect on the overall properties of the composite. It is noted that the fast multipole BEM prediction shows good agreement with the analytical solution. Figures 7 and 8 give the effect of the interface parameters on the average strain when E_f=1 Mpa and E_f=100 MPa for the Burgers model. The corresponding average strain increases with the decrease of the interface parameters. It indicates that a stiff inclusion surrounded by a weak interface behaves as a soft inclusion.

Figure 9 plots the effects of the interface parameters and volume content on the creep compliance of the composite. For a weak interface, the corresponding creep compliance increases with the increase of the volume content of the inclusions. This indicates that with a weaker interface, the material with the higher volume content will creep faster. The reason is that more inclusions will act as cavities when the rigidity of the interface tends to zero. Therefore, the composite is softer even than the non-reinforced matrix. On the contrary, when the interface parameters are relatively

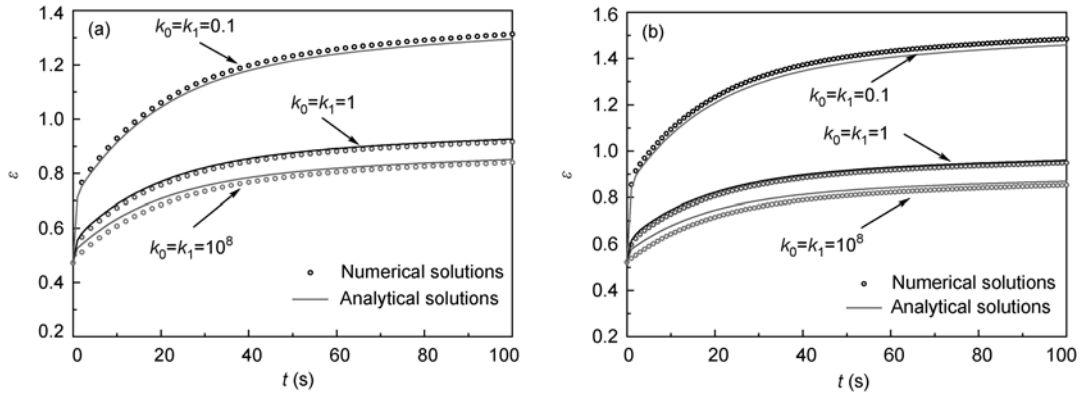

Figure 7 Comparison of the average strains between the numerical and analytical solutions when E_f=1 MPa for Type 2 model. (a) Volume fraction f=0.3; (b) volume fraction f=0.4.

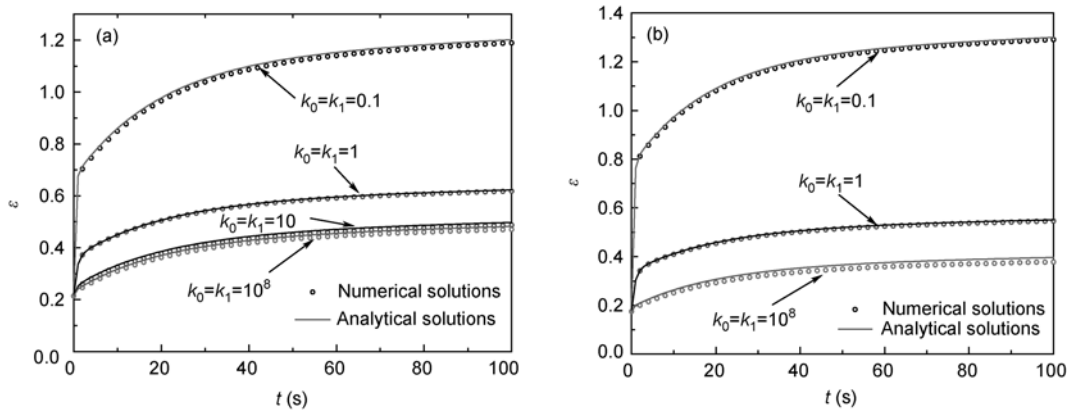

Figure 8 Comparison of the average strains between the numerical and analytical solutions when E_f=100 MPa for Type 1 model. (a) Volume fraction f=0.3; (b) volume fraction f=0.4.

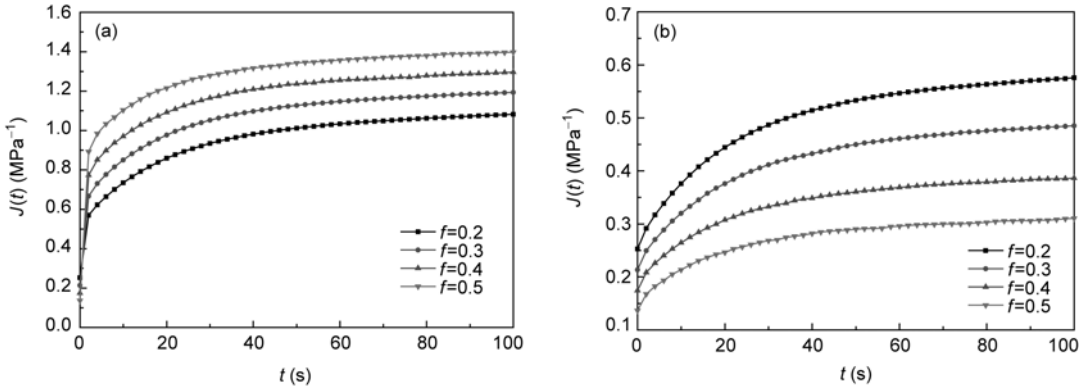

Figure 9 The creep compliance curves for various volume fractions. (a) k_0=k_1=0.1 MPa/m; (b) k_0=k_1=10 MPa/m.

large, the material with the lower volume content will creep faster. This conclusion agrees well with the concept of reinforced composites.

4.3 Numerical implementation for asphalt concrete modeling

Asphalt concrete is widely used in the surface layer of flexible pavements. It is a typical complex composite made of aggregates, asphalt binder, air voids and additives. At low temperature, asphalt concrete can be treated as an elastic body, while at high temperature, it presents apparent viscoelastic characteristic. Therefore, it is necessary to start with an assessment of their viscoelastic material properties such as creep compliance or relaxation modulus to explain the mechanical influence of fillers on the asphalt mixtures. The purpose of this study is to predict the asphalt concrete creep compliance with the developed viscoelastic simulation tool on a cross-sectional image model. This numerical prediction will be compared with the creep test results from laboratory asphalt concrete specimens.

First, the cross-sectional images of the asphalt concrete samples are developed for numerical modeling. Since it is impossible to identify aggregates that are very small, the model is assumed to be composed of two phases only [33]. The first phase is the mastic, which consists of fine aggregates (taken as aggregates passing 2.36 mm sieve), sands, fines and asphalt binder. The other phase is the coarse aggregates larger than 2.36 mm sieve. Figure 10(a) shows a real sample from a sectional surface of the asphalt concrete specimen, and Figure 10(b) presents the fitted elliptical

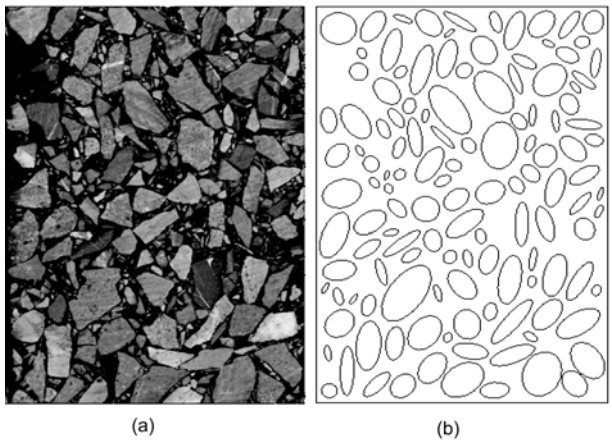

Figure 10 Asphalt concrete image model generation for FMBEM simulation. (a) Original sample; (b) fitted elliptical aggregates sample.

aggregates model by means of image processing technique. The center coordinates, the area, orientation and long axis of the aggregates are determined firstly, and then the short axis is figured out according to the area and long axis of each ellipse. Therefore, the developed model has the same volume content as the actual sample.

The time-dependent creep compliance of the mastic is approximated by the two Voigt+one spring type models and the parameters of this model can be determined by fitting the experimental data of creep test. The 3-point bending test has been conducted to determine the relaxation modulus of the mastic and asphalt concrete. The relaxation modulus and time values for the mastic are listed in Table 1. The uniaxial compression is applied on the top and bottom layer. Therefore, the creep compliance of the asphalt concrete can be obtained according to eq. (64). It is noted that we have no experimental results of relaxation modulus from the uniaxial compression test at this time. However, relaxation modulus is a fundamental material property. Therefore, the viscoelastic properties of mastic and asphalt concrete from different test methods are comparable, as adopted by other researchers [34]. The plane stress condition is considered in the present study.

The creep tests are performed on samples to determine the time-dependent behavior of the asphalt concrete and the results are used to compare with the FMBEM analysis. For each composition, three samples are made and tested. For instance, in Figure 11, they are represented as Samples A, B and C. Figure 11 shows a comparison between the experimental and computational results with elliptical aggregates sample. Here, the interface imperfection parameters are gained as $k_0=k_1=5$ MPa/m by fitting the experiment results. The viscoelastic response obtained by FMBEM matches quite well with the rising part of the experimental curve (Sample C) and matches well with the stable part of the experimental curve (Sample A), and its middle part is located between Samples A and C. Therefore, this proposed elliptical aggregate sample with the developed FMBEM is adequate to predict the global viscoelastic behavior of the asphalt concrete.

Table 1 Two Voigt+one spring model parameters for the mastic

E_0 (MPa)	E_1 (MPa)	E_2 (MPa)	η_1 (MPa·min)	η_1 (MPa·min)
298.5	10.3	1.7	27.17	51.32

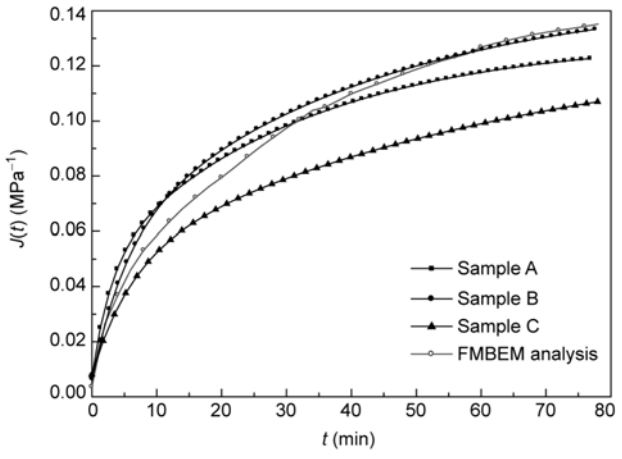

Figure 11 Comparison of asphalt concrete creep compliance between experimental and FMBEM results.

5 Conclusion

A fast multipole BEM analysis for solving 2D linear viscoelastic multi-inclusion problems with the presence of imperfect viscoelastic interfaces is presented in this paper. Systems of the multipole expansion equations are formed and solved numerically by incorporating the time domain method. The Kelvin model is introduced to simulate the interface imperfection. The interaction among inclusions as well as elimination of the phenomenon of material penetration is also considered. Since the transformed multipole formulations are identical to those for the 2D elastic problems, it is quite easy to implement the 2D viscoelastic fast multipole boundary element method.

Two numerical examples, including planar viscoelastic composites with single inclusion or randomly distributed multi-inclusions, are given to demonstrate the accuracy, efficiency, and versatility of the developed FMBEM. Results also show that the interface properties, volume ratio and stiffness of inclusions, as well as the viscoelastic characteristic of the matrix have significant effect on the creep behavior of linear viscoelastic materials. For examples, for a weaker interface, the particle-reinforced composites with the higher volume content will creep faster, while for a stronger interface, the material with the lower volume content will creep faster. Finally, the focus is placed on implementation of the approach to investigate the viscoelastic characteristic of the asphalt concrete. The results indicate that the proposed elliptical aggregate sample with the developed FMBEM is applicable for asphalt concrete creep compliance prediction. In general, the advantage of FMBEM in higher speed and lower storage makes it possible to deal with many potential application problems, especially for multi-time step problems (e.g. the viscoelastic case).

Further investigations will be carried out to extend the present fast multipole BEM for viscoelastic problem from 2D to 3D. Besides, the consideration of the interface cracks in the present FMBEM simulation will be an interesting topic and can be carried out readily. Therefore, it is possible to make use of this method to study many engineering materials, such as polymers, composites, non-ferrous metals, rocks, concrete and others in the near future.

The work was supported by the National Natural Science Foundation of China (Grant No. 10725210) and the National Basic Research Program of China (Grant No. 2009CB623200).

1 Rizzo F J, Shippy D J. An application of the correspondence principle of linear viscoelasticity theory. J Appl Math, 1971, 21: 321–330
2 Kusama T, Mitsui Y. Boundary element method applied to linear viscoelastic analysis. Appl Math Modelling 1982; 6: 285–294
3 Sun B N, Hsiao C C. Viscoelastic boundary method for analysing polymer quasi fracture. Comput Struct, 1988, 30: 963–966
4 Liu Y, Antes H. Application of visco-elastic boundary element method to creep problems in chemical engineering structures. Int J Pres Ves & Piping, 1997, 70: 27–31
5 Tschoegl N W. The Phenomenological Theory of Linear Viscoelastic Behavior: An Introduction. New York: Springer, 1989
6 Mesquita A D, Coda H B, Venturini W S. An alternative time marching process for viscoelastic analysis by BEM and FEM. Int J Numer Meth Eng, 2001, 51: 1157–1173
7 Mesquita A D, Coda H B. An alternative time integration procedure for Boltzmann viscoelasticity: a BEM approach. Comput Struct, 2001, 79/16: 1487–1496
8 Mesquita A D, Coda H B. Boundary integral equation method for general viscoelastic analysis. Int J Solids Struct, 2002, 39: 2643–2664
9 Mesquita A D, Coda H B. A simple Kelvin and Boltzmann viscoelastic analysis of three-dimensional solids by the boundary element method. Engng Anal Bound Elem, 2003, 27: 885–895
10 Huang Y, Steven L C, Sofia G M. A time domain direct boundary integral method for a viscoelastic plane with circular holes and elastic inclusions. Engng Anal Bound Elem, 2005, 29: 725–737
11 Sensale B, Greus G J. Boundary element analysis of viscoelastic fracture. In: Brebbia C A, Rencis J J, eds. Bounday Element XV, vol. 2. Stress Analysis. Boston: Computational Mechanics Publication, 1993
12 Sensale B. On the solution of viscoelastic problems using boundary elements techniques. Doctoral Dissertation, CEMACOM, UFRGS, Porto Alegre, Portuguese, 1997
13 Sensale B, Partridge P W, Creus G J. General boundary elements solution for aging viscoelastic structures. Int J Numer Meth Eng, 2001, 50: 1455–1468
14 Birgisson B, Sangpetngam B, Roque R. Prediction of the viscoelastic response and crack growth in asphalt mixtures using the boundary element method. Transp Res Rec, 2002, 1789: 129–135
15 Birgisson B, Soranakom C, Napier J A L, et al. Microstructure and fracture in asphalt mixtures using a boundary element approach. J Mater Civ Eng, 2004, 16: 116–121
16 Wang J L, Birgisson B. A time domain boundary element method for modeling the quasi-static viscoelastic behavior of asphalt pavements. Engng Anal Bound Elem, 2007, 31: 226–40
17 Lane F, Leguillon D. Homogenized constitutive law for a partially cohesive composite material. Intl J Solids Struct, 1982, 18: 443–458
18 Greengard L F, Kropinski M C, Mayo A. Integral equation methods for Stokes flow and isotropic elasticity in the plane. J Comput Phys, 1996, 125: 403–414
19 Greengard L F, Helsing J. On the numerical evaluation of elastostatic fields in locally isotropic two-dimensional composites. J Mech Phys Solids, 1998, 46: 1441–1462
20 Peirce A P, Napier J A L. A spectral multipole method for efficient solution of large-scale boundary element models in elastostatics. Int J Numer Meth Eng, 1995, 38: 4009–4034
21 Yao Z, Kong F, Wang H, et al. 2D simulation of composite materials using BEM. Engng Anal Bound Elem, 2004, 28: 927–935
22 Wang H, Yao Z, Wang P. On the preconditioners for fast multipole boundary element methods for 2D multi-domain elastostatics. Engng Anal Bound Elem, 2005, 29: 673–688
23 Liu Y J, Nishimura N, Otani Y. Large-scale modeling of carbon-nanotube composites by the boundary element method based on a rigid-inclusion model. Comput Mater Sci, 2005, 34: 173–187
24 Liu Y J. A new fast multipole boundary element method for solving large-scale two-dimensional elastostatic problems. Int J Numer Meth Eng, 2005, 65: 863–881
25 Liu Y J, Nishimura N, Otani Y, et al. A fast boundary element method for the analysis of fiber-reinforced composites based on a rigid-inclusion model. J Appl Mech, 2005, 72: 115–128
26 Liu Y J. A fast multipole boundary element method for 2-D multi-domain elastostatic problems based on a dual BIE formulation. Comput Mech, 2008, 42: 761–773
27 Liu Y J. Fast Multipole Boundary Element Method—Theory and Applications in Engineering. Cambridge: Cambridge University Press, 2009
28 Chen W Q, Zhu X Y, Huang Z Y. Modeling of multi-inclusion composites with interfacial imperfections: Micromechanical and numerical simulations. Sci China Ser E-Tech Sci, 2010, 53(3): 720–730
29 Lee S S, Westmann RA. Application of boundary element method to visco-elastic problems. In: Brebbia C A, Rencis J J. eds. Boundary Element XV, vol 2, Stress Analysis. Boston: Computational Mechanics Publications, 1993
30 Lee S S. Boundary element analysis of linear viscoelastic problems using realistic relaxation functions. Comput Struct, 1995, 55(6): 1027–1036
31 Achenbach J D, Zhu H. Effect of interfacial zone on mechanical behavior and failure of fiber-reinforced composites. J Mech Phys Solids, 1989, 37(3): 381–393
32 Hu N, Wang B, Tan GW, Yet al. Effective elastic properties of 2D solids with circular holes: numerical simulations. Compos Sci Tech, 2000, 60: 1184–1123
33 Ranja B, Animesh D, Sumit B. Numerical simulation of mechanical behavior of asphalt mix. Constr Build Mater, 2008, 22: 1051–1058
34 Dai Q L, You Z P. Prediction of creep stiffness of asphalt mixture with micromechanical finite-element and discrete-element models. J Eng Mech-ASCE, 2007, 2: 163–173